Synchronized Firings in the Networks of Class 1 Excitable Neurons with Excitatory and Inhibitory Connections and their Dependences on the Forms of Interactions

Takashi Kanamaru and Masatoshi Sekine

Department of Electrical and Electronic Engineering, Faculty of Technology, Tokyo University of Agriculture and Technology, Tokyo 184-8588, Japan

Related Java Simulator:
http://brain.cc.kogakuin.ac.jp/~kanamaru/Chaos/e/sC1CFP/
(If you prefer Japanese version, please omit "e/" in the URL.)

Abstract

Synchronized firings in the networks of class 1 excitable neurons with excitatory and inhibitory connections are investigated, and their dependences on the forms of interactions are analyzed. As the forms of interactions, we treat the double exponential coupling and the interactions derived from it, namely, the pulse-coupling, the exponential coupling, and the alpha-coupling. It is found that the bifurcation structure of the networks mainly depends on the decay time of the synaptic interaction and the effect of the rise time is smaller than that of the decay time.

Keywords

class 1 excitable neuron, excitatory neuron, inhibitory neuron, synchronization, periodic firing, chaos, Fokker-Planck equation, rise/decay time

1 Introduction

Recently, oscillations and synchronization in neural systems are attracting considerable attention. Particularly, in the visual cortex and the hippocampus, synchronized oscillations with typical frequencies are often observed in the average behaviors of the neuronal ensemble, and it is proposed that they are related to the binding of the information in the visual cortex, and the regulation of the synaptic plasticity in the hippocampus (for a review, see Gray (1994)).

To understand the mechanism of such synchronized oscillations, networks of excitatory or inhibitory neurons have been investigated by numerous authors (Abbott and Vreeswijk, 1993; Hansel, Mato, and Meunier, 1995; Kuramoto, 1991; Mirollo and Strogatz, 1990; Sato and Shiino, 2002; Tsodyks, Mitkov, and Sompolinsky, 1993; van Vreeswijk, 1996; van Vreeswijk, Abbott and Ermentrout, 1994). Typically, the perfect

synchronization is observed in the network of pulse-coupled self-oscillating excitatory neurons (Kuramoto, 1991; Mirollo and Strogatz, 1990), but it is not always stable for networks with slow couplings, and the partial synchronization, the anti-phase synchronization, or an asynchronous state appears depending on the parameters such as the characteristic time scale of the synaptic interaction (Abbott and Vreeswijk, 1993; Hansel, Mato, and Meunier, 1995; Sato and Shiino, 2002; Tsodyks, Mitkov, and Sompolinsky, 1993; van Vreeswijk, 1996; van Vreeswijk, Abbott and Ermentrout, 1994). The frequencies of these synchronized firings are determined mainly by the frequency of a single neuron, and they might be much larger than the physiologically observed ones, such as 40Hz of the gamma oscillation.

Recently, more complex dynamics than that of the excitatory network have been found in networks of excitatory and inhibitory neurons (Börgers and Kopell, 2003; Brunel, 2000; Golomb and Ermentrout, 2001; Hansel and Mato, 2003; Kanamaru and Sekine, 2003, 2004; van Vreeswijk and Sompolinsky, 1996). Similarly to the excitatory network, the synchronized firings are observed in the network of self-oscillating neurons (Börgers and Kopell, 2003) or in the network of self-oscillating and excitable neurons (Hansel and Mato, 2003). Moreover, the synchronized firings are observed even in the network only of excitable neurons with excitatory and inhibitory connections under noisy environment (Brunel, 2000; Kanamaru and Sekine, 2003, 2004), where excitable neurons in the absence of connections fire randomly with the help of noise, and when an appropriate strength of connections is introduced, the synchronized firings appear. In our previous studies (Kanamaru and Sekine, 2003, 2004), a noisy network of class 1 neurons with excitatory and inhibitory connections is investigated by

means of bifurcation analyses, and various synchronized firings including chaotic ones are found. It is found that the frequencies of such synchronized firings depend on both the noise intensity and the coupling strength. In this model, the characteristic time scale of the interaction is assumed to be the same order as that of each neuron, and we could not examine the effect of the time scale of synaptic interactions systematically.

In the present paper, we investigate the synchronized firings in the networks of class 1 excitable neurons with excitatory and inhibitory connections under noisy environment, and examine their dependences on the forms of interactions. As the forms of interactions, we treat the double exponential coupling and the interactions derived from it in some limiting cases, namely, the pulse-coupling, the exponential coupling, and the alpha-coupling. With these couplings, the dependence of the bifurcation structure on the rise time and the decay time of synaptic interactions is investigated. In section 2, the definition of our model is given and its Fokker-Planck equations are introduced. Four forms of interactions, namely, the double exponential coupling, the pulse-coupling, the exponential coupling, and the alpha-coupling are also introduced. In section 3, the network with the pulse-coupling is analyzed by solving the Fokker-Planck equations, and a bifurcation set is obtained numerically. It is observed that the synchronized periodic firings appear mainly by going through the Hopf bifurcation or the saddle-node on limit cycle bifurcation. In section 4, the network with the exponential coupling is analyzed. Besides the synchronized periodic firings, synchronized chaotic firings and anomalous high-frequency synchronization are observed. The effect of the decay time of the synaptic interaction is also investigated. In section 5, the networks with the alpha-coupling or the double exponential coupling are analyzed. It is found that the dependence of the bifurcation structure on the rise time of the synaptic interaction is weaker than that on the decay time. Conclusions and discussions are given in the final section.

2 Model

Let us consider the coupled active rotators composed of excitatory neurons $\theta_E^{(i)}$ ($i = 1, 2, \cdots, N_E$) and inhibitory neurons $\theta_I^{(i)}$ ($i = 1, 2, \cdots, N_I$) (Kanamaru and Sekine, 2003, 2004) written as

$$
\begin{aligned}
\tau_E \dot{\theta}_E^{(i)} &= 1 - a \sin \theta_E^{(i)} + \xi_E^{(i)}(t) \\
&\quad + I_{EE}(t) - I_{EI}(t), \qquad (2.1) \\
\tau_I \dot{\theta}_I^{(i)} &= 1 - a \sin \theta_I^{(i)} + \xi_I^{(i)}(t)
\end{aligned}
$$

$$
+ I_{IE}(t) - I_{II}(t). \qquad (2.2)
$$

Here, a is a system parameter, τ_E and τ_I are the time constants of the neuron, $I_{XY}(t)$ ($X, Y = E$ or I) is the synaptic input from the ensemble Y to the ensemble X, and $\xi_X^{(i)}(t)$ is Gaussian white noise satisfying

$$
\langle \xi_X^{(i)}(t) \xi_Y^{(j)}(t') \rangle = D \delta_{ij} \delta_{XY} \delta(t - t'), \qquad (2.3)
$$

where D is the noise intensity and δ_{ij} is Kronecker's delta. For $a > 1$, an active rotator shows typical properties of an excitable system, namely, it has a stable equilibrium $\theta_0 \equiv \arcsin(1/a)$, and $-\sin(\theta^{(i)}(t)) + 1/a$ shows a pulse-like waveform when an appropriate amount of disturbance is injected (Kurrer and Schulten, 1995; Sakaguchi, Shinomoto, and Kuramoto, 1988; Shinomoto and Kuramoto, 1986; Tanabe, Shimokawa, Sato, and Pakdaman, 1999). Note that a single active rotator can be transformed into the canonical model $\dot{\theta} = (1 - \cos\theta) + (1 + \cos\theta)r$ for class 1 neurons (Ermentrout, 1996; Izhikevich, 1999). Thus, our synaptically coupled active rotators might reflect the dynamics of networks of class 1 neurons such as Connor model or Morris-Lecar model (Ermentrout, 1996). Moreover, the active rotator has a property that its Fokker-Planck equations can be numerically integrated with smaller number of terms than that of the leaky integrate-and-fire model. Thus, we consider it as an effective tool to analyze the dynamics of pulse neural networks.

As the interaction $I_{XY}(t)$ from the ensemble Y to the ensemble X ($X, Y = E$ or I), we consider the difference of two exponential functions (Abbott and Vreeswijk, 1993; Hansel, Mato, and Meunier, 1995; Gerstner and Kistler, 2002) written as

$$
\begin{aligned}
I_{XY}(t) = \frac{g_{XY}}{N_Y} \sum_{j=1}^{N_Y} \sum_k \frac{1}{\kappa_{1Y} - \kappa_{2Y}} \\
\times \left\{ \exp\left(-\frac{t - t_k^{(j)}}{\kappa_{1Y}} \right) - \exp\left(-\frac{t - t_k^{(j)}}{\kappa_{2Y}} \right) \right\},
\end{aligned}
$$
$$
\qquad (2.4)
$$

where $t_k^{(j)}$ is the k-th firing time of the j-th neuron, and κ_{1Y} and κ_{2Y} ($\kappa_{1Y} > \kappa_{2Y} > 0$) denote the decay time and the rise time of the synaptic interaction, respectively. Note that the second sum is taken over k satisfying $t > t_k^{(j)}$, and the firing time is defined as the time when $\theta_Y^{(j)}$ turns around over the value $3\pi/2$ which is the point located at the opposite side of the stable equilibrium point $\theta_0 = \arcsin(1/a) \sim \pi/2$. This interaction is called the double exponential coupling in the following.

In the three limits $\kappa_{1Y}, \kappa_{2Y} \to 0$, $\kappa_{2Y} \to 0$ ($\kappa_{1Y} \equiv \kappa_Y$), and $\kappa_{1Y} \to \kappa_{2Y} \equiv \kappa_Y$, $I_{XY}(t)$ is rewritten as

$$I_{XY}(t) = \frac{g_{XY}}{N_Y} \sum_{j=1}^{N_Y} \sum_k \delta(t - t_k^{(j)}), \qquad (2.5)$$

$$I_{XY}(t) = \frac{g_{XY}}{N_Y} \sum_{j=1}^{N_Y} \sum_k \frac{1}{\kappa_Y} \exp\left(-\frac{t - t_k^{(j)}}{\kappa_Y}\right), \qquad (2.6)$$

$$I_{XY}(t) = \frac{g_{XY}}{N_Y} \sum_{j=1}^{N_Y} \sum_k \frac{t - t_k^{(j)}}{\kappa_Y^2} \exp\left(-\frac{t - t_k^{(j)}}{\kappa_Y}\right), \qquad (2.7)$$

and we call them the pulse-coupling, the exponential coupling, and the alpha-coupling, respectively. In the following, synchronization phenomena in the network with each coupling are analyzed. To reduce the number of parameters, we set $g_{EE} = g_{II} \equiv g_{int}$, $g_{EI} = g_{IE} \equiv g_{ext}$, $a = 1.05$, and $\tau_E = \tau_I = 1.0$.

In the previous studies (Kanamaru and Sekine, 2003, 2004), we considered a network with the waveform-coupling written as

$$I_{XY}(t) = \frac{g_{XY}}{N_Y} \sum_{j=1}^{N_Y} (-\sin\theta_Y^{(j)} + 1/a), \qquad (2.8)$$

where the waveform of the pulse is injected to the next neuron directly, and found various synchronized firings including the synchronized chaotic firings and the weakly synchronized periodic firings. It is noticeable that chaos is observed in the noisy network of active rotators, while chaos does not appear in a single active rotator by the general property of one dimensional differential equations. In those studies, the waveform-coupling was used for the facilitation of the numerical analyses, but, to compare them with the physiologically observed synchronization phenomena, the double exponential coupling and the couplings derived from it seem to be more appropriate.

For the analysis, let us introduce the Fokker-Planck equations (Gerstner and Kistler, 2002; Kuramoto, 1984)

$$\frac{\partial n_E}{\partial t} = -\frac{1}{\tau_E} \frac{\partial}{\partial \theta_E} (A_E n_E) + \frac{D}{2\tau_E^2} \frac{\partial^2 n_E}{\partial \theta_E^2}, \qquad (2.9)$$

$$\frac{\partial n_I}{\partial t} = -\frac{1}{\tau_I} \frac{\partial}{\partial \theta_I} (A_I n_I) + \frac{D}{2\tau_I^2} \frac{\partial^2 n_I}{\partial \theta_I^2}, \qquad (2.10)$$

$$A_E(\theta_E, t) = 1 - a\sin\theta_E + I_{EE}(t) - I_{EI}(t), \qquad (2.11)$$

$$A_I(\theta_I, t) = 1 - a\sin\theta_I + I_{IE}(t) - I_{II}(t), \qquad (2.12)$$

for the normalized number densities of the excitatory and inhibitory neurons

$$n_E(\theta_E, t) \equiv \frac{1}{N_E} \sum \delta(\theta_E^{(i)} - \theta_E), \qquad (2.13)$$

$$n_I(\theta_I, t) \equiv \frac{1}{N_I} \sum \delta(\theta_I^{(i)} - \theta_I), \qquad (2.14)$$

in the limit $N_E, N_I \to \infty$. Note that asynchronous firings and synchronized firings of the network correspond to a stationary solution and a time-varying solution of the Fokker-Planck equations, respectively.

The probability fluxes for the excitatory and inhibitory ensembles are defined as

$$J_E(\theta_E, t) = \frac{1}{\tau_E} A_E n_E - \frac{D}{2\tau_E^2} \frac{\partial n_E}{\partial \theta_E}, \qquad (2.15)$$

$$J_I(\theta_I, t) = \frac{1}{\tau_I} A_I n_I - \frac{D}{2\tau_I^2} \frac{\partial n_I}{\partial \theta_I}, \qquad (2.16)$$

respectively. Note that the probability flux at $\theta = 3\pi/2$ can be interpreted as the instantaneous firing rate at t for each ensemble.

3   Pulse-coupling

In this section, a network with the pulse-coupling written by equations 2.1, 2.2, and 2.5 is considered.

The coupling term $I_{XY}(t)$ in equation 2.5 is approximated as

$$I_{XY}(t) = g_{XY} J_Y(t) + \sigma(t), \qquad (3.1)$$

where $J_Y(t) \equiv J_Y(3\pi/2, t)$ is the firing rate, and $\sigma(t)$ is a fluctuation term. The probability flux $J_Y(t)$ at $\theta = 3\pi/2$ is obtained by solving equations 2.15 and 2.16 for $\theta = 3\pi/2$. This flux $J_Y(t)$ can be calculated when an inequality

$$\left(1 - \frac{g_{EE}}{\tau_E} n_E\left(\frac{3\pi}{2}\right)\right) \left(1 + \frac{g_{II}}{\tau_I} n_I\left(\frac{3\pi}{2}\right)\right)$$
$$+ \frac{g_{EI} g_{IE}}{\tau_E \tau_I} n_E\left(\frac{3\pi}{2}\right) n_I\left(\frac{3\pi}{2}\right) \neq 0 \qquad (3.2)$$

is satisfied. A sufficient condition for inequality 3.2 is

$$1 - \frac{g_{EE}}{\tau_E} n_E\left(\frac{3\pi}{2}\right) > 0 \qquad (3.3)$$

because the other terms in 3.2 are positive. Within all our numerical solutions, the condition 3.3 is proven to be satisfied.
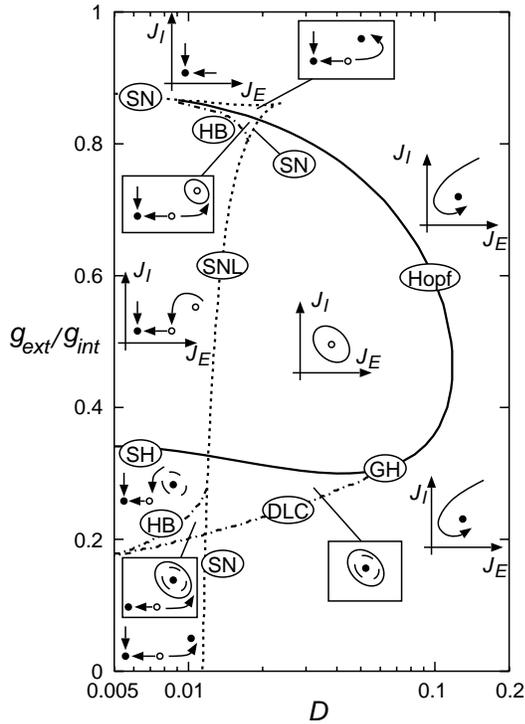
Figure 1: A bifurcation set in the (D, g_{ext}) plane for the pulse-coupled network with $g_{int} = 3.5$. The solid, dotted, and dash-dotted lines denote the Hopf, saddle-node, and global bifurcations, respectively. Schematic flows of the solution in the (J_E, J_I) plane are also drawn on the bifurcation set. The filled and open circles in the trajectories in the (J_E, J_I) plane denote the stable and unstable equilibrium points, respectively. And the solid and dashed closed curves denote the stable and unstable limit cycles, respectively. The meanings of the abbreviations are as follows: SN, saddle-node; SNL, saddle-node on limit cycle; DLC, double limit cycle; HB, homoclinic bifurcation; SH, subcritical Hopf; GH, generalized Hopf.

In the limit of $N_Y \to \infty$, the fluctuation term $\sigma(t)$ converges to zero. With this approximation, a numerically obtained bifurcation set for $g_{int} = 3.5$ in the (D, g_{ext}) plane is shown in Figure 1. Typically, there exist synchronized firings in the area between the Hopf bifurcation line and the saddle-node on limit cycle bifurcation line with moderate values of D. In Figure 1, flows in the plane of probability fluxes J_E and J_I are also shown, and their explanations are given in the latter half of this section. The Hopf and the saddle-node bifurcation lines are obtained as follows. First, equations 2.9 and 2.10 are transformed into a set of ordinary differential equations $\dot{\boldsymbol{x}} = \boldsymbol{f}(\boldsymbol{x})$ for the spatial

Fourier coefficients of n_E and n_I as shown in the Appendix. Next a stationary solution $\boldsymbol{x}_0$ is numerically obtained with the Newton method (Press et al., 1988), and the eigenvalues of the Jacobian matrix $D\boldsymbol{f}(\boldsymbol{x}_0)$ numerically obtained by using the QR algorithm (Press et al., 1988) are examined to find bifurcation lines. For numerical calculations, each Fourier series is truncated at the first 40 or 60 terms.

The homoclinic and the double limit cycle bifurcation lines are obtained by observing the long time behaviors of the solutions of equations 2.9 and 2.10. This bifurcation set is similar to that of the network with the waveform-coupling (Kanamaru and Sekine, 2003) except the fact that chaotic firings found in the network with the waveform-coupling does not exist in this network.

To understand the bifurcation set, schematic flows of the solution in the (J_E, J_I) plane are also drawn on the bifurcation set in Figure 1. Note that a stationary solution and a time-periodic solution of the Fokker-Planck equations are projected as an equilibrium point and a limit cycle onto the (J_E, J_I) plane, respectively, and they correspond to the asynchronous and the synchronized firings of the network, respectively. Typically, for small D and moderate g_{ext}, there exist a stable equilibrium point with small probability fluxes. This equilibrium point corresponds to the firings where all neurons fluctuate around their resting potentials, and, when this point disappears by the saddle-node on limit cycle bifurcation, the synchronized firings appear. For large D, there exist a stable equilibrium point with large probability fluxes, and it corresponds to the firings where neurons fire with high frequencies without correlations. And the synchronized firings also appear after the Hopf bifurcation of the equilibrium point. This equilibrium point approaches to the origin of the (J_E, J_I) plane with the increase of g_{ext}, and its probability fluxes become small. Moreover, in some region in the bifurcation set, the synchronized firings also appear by the double limit cycle bifurcation or the homoclinic bifurcation. For more information about each bifurcation, see Guckenheimer and Holmes (1983); Hoppensteadt and Izhikevich (1997).

The raster plots of the typical synchronized firings for the finite system with $N_E = N_I = 1000$ are shown in Figure 2. Each figure shows the firing times of the neurons. As shown in Figure 2A, the synchronized firings near the saddle-node on limit cycle bifurcation have a long period and their degree of synchronization is strong. This is because the system stays long time in the area where the original saddle and node existed. As shown in Figure 2B, the synchronized firings near the Hopf bifurcation have a short period and their degree of synchronization is weak. This is be-
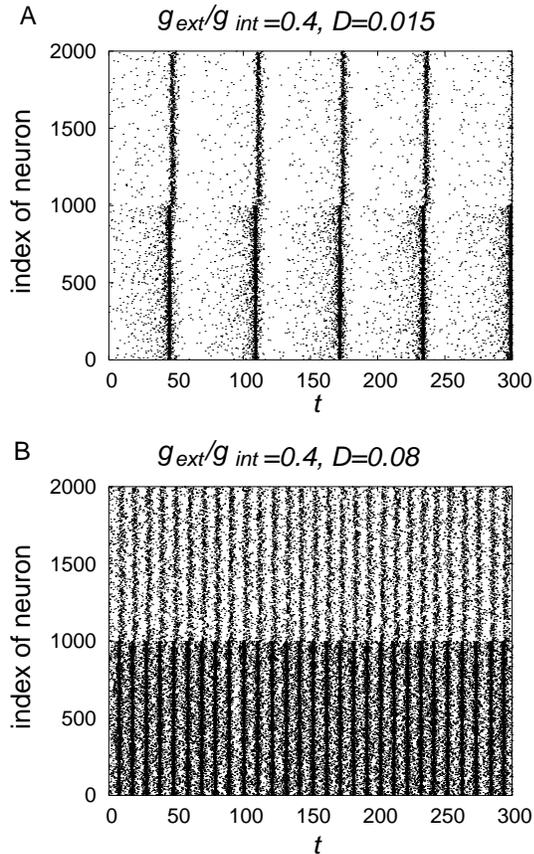
Figure 2: The raster plots of the typical synchronized firings for the finite system with $N_E = N_I = 1000$. The parameters are set at (A) $g_{ext}/g_{int} = 0.4$ and $D = 0.015$, and (B) $g_{ext}/g_{int} = 0.4$ and $D = 0.08$ with $g_{int} = 3.5$. The neurons are aligned so that the excitatory neurons are in the range $0 \leq i < 1000$ and the inhibitory neurons are in the range $1000 \leq i < 2000$.

cause the limit cycle which corresponds to this weakly synchronized firing with a high firing rate is created around the stable equilibrium point which denotes the asynchronous firings.

4   Exponential coupling

In this section, a network with the exponential coupling is analyzed. The parameters are fixed at $\kappa_E = \kappa_I = 1$ and $g_{int} = 3.5$.

For large number of neurons, equation 2.6 is approximated by the Ornstein-Uhlenbeck process (Gardiner, 1985) written as

$$\dot{I}_{XY}(t) = -(I_{XY}(t) - g_{XY}J_Y(t))/\kappa_Y + \sigma(t), \quad (4.1)$$

where $\sigma(t)$ is a fluctuation term, and $\sigma(t)$ converges to zero in the limit of $N_Y \to \infty$. By integrating this differential equation with the Fokker-Planck equations, the exponentially coupled network can be numerically analyzed. A numerically obtained bifurcation set in the (D, g_{ext}) plane is shown in Figure 3. In this bi-
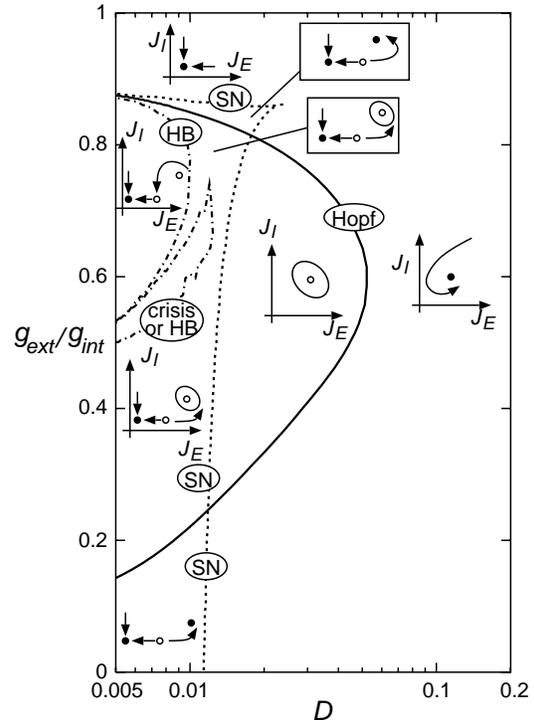
Figure 3: A numerically obtained bifurcation set of the exponentially coupled network. The parameters are set at $\kappa_E = \kappa_I = 1$ and $g_{int} = 3.5$. The solid, dotted, and dash-dotted lines denote the Hopf, saddle-node, and global bifurcations, respectively. Schematic flows of the solution in the (J_E, J_I) plane are also drawn on the bifurcation set. The filled and open circles in the trajectories in the (J_E, J_I) plane denote the stable and unstable equilibrium points, respectively. And the solid closed curves denote the stable limit cycle. The meanings of the abbreviations are as follows: SN, saddle-node; HB, homoclinic bifurcation.

furcation set, there exists a crisis line where a chaotic solution disappears, as it will be explained later in this section.

In Figure 3, schematic flows of the solution in the (J_E, J_I) plane are also drawn on the bifurcation set. The bifurcation structure roughly resembles that of the pulse-coupled network, but, in the exponentially coupled network, there additionally exist the period-doubling bifurcations and the chaotic solutions.

5

The flows in the (J_E, J_I) plane, the time series of J_E, and the raster plots for the finite system with $N_E = N_I = 1000$ are shown in Figures 4A, B, and C, respectively, and the synchronized chaotic firings are observed. Let us consider the Poincaré section of
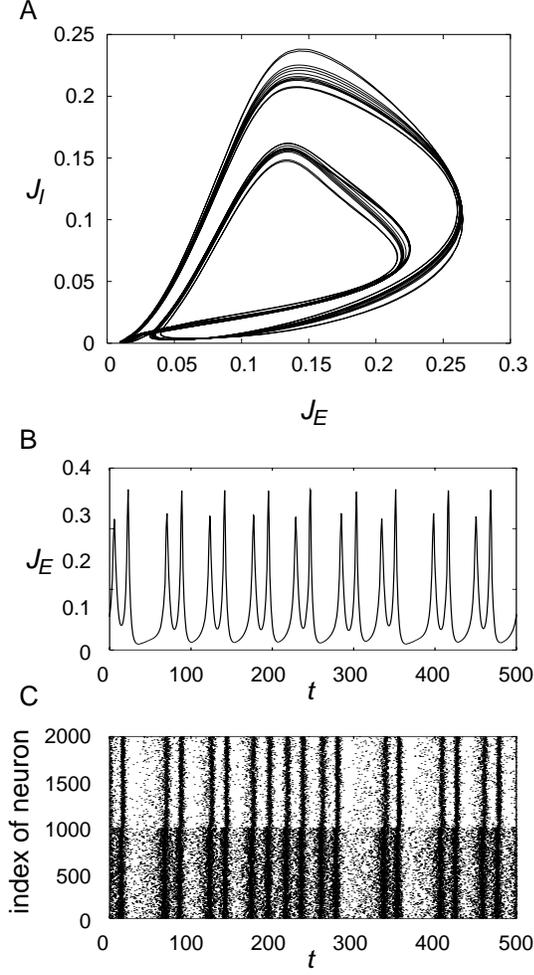
Figure 4: The chaotic dynamics observed in the exponentially coupled network for $g_{ext}/g_{int} = 0.64$, $g_{int} = 3.5$, and $D = 0.0125$. (A) A flow in the (J_E, J_I) plane. (B) A time series of J_E. (C) The raster plot of the firings in the finite system with $N_E = N_I = 1000$.

the trajectory at a line $J_E = 0.15$ with $dJ_E/dt > 0$ in the (J_E, J_I) plane. The bifurcation diagram of the attractors at the Poincaré section against D for $g_{ext}/g_{int} = 0.64$ and $g_{int} = 3.5$ is shown in Figure 5A, and the chaotic attractors are observed. To confirm that the chaotic behaviors in Figure 5A are actually chaotic, the largest Lyapunov exponent is calculated by the standard technique (Ott, 1993), namely, by calculating the expansion rate of two nearby trajectories
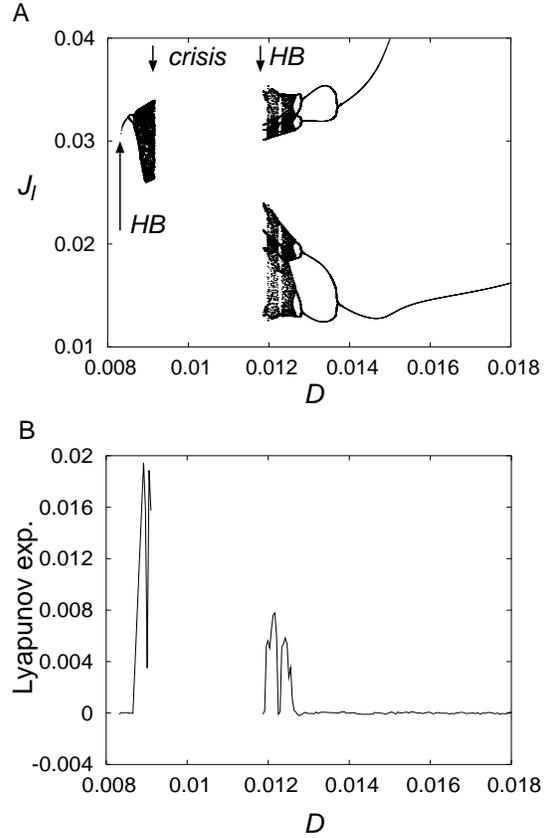
Figure 5: The positions of the attractors on the Poincaré section $J_E = 0.15$ against D for $g_{ext}/g_{int} = 0.64$. (B) The corresponding Lyapunov exponent.

each of which follows a set of ordinary differential equations $\dot{\boldsymbol{x}} = \boldsymbol{f}(\boldsymbol{x})$ for the spatial Fourier coefficients of equations 2.9 and 2.10. The corresponding Lyapunov exponent is shown in Figure 5B. It is observed that the Lyapunov exponent takes positive values when the chaotic solutions exist, and takes zero when periodic solutions are stable.

In the following, periodic solutions with the period n in the Poincaré section are called periodic solutions with cycle n. The areas where the periodic solutions with cycle 2 or 4, or the chaotic solutions exist are roughly sketched in Figure 6. The periodic solutions with large cycles and the windows in the chaotic regions are neglected because their areas are very narrow. In the bifurcation set, there exist points of crisis line where the chaotic attractors disappear. When a periodic solution instead of the chaotic attractor disappears, this point is the point of homoclinic bifurcation.

For small g_{ext}, high-frequency synchronization where excitatory neurons continue to fire with the period about their pulse width are observed. The flows

6
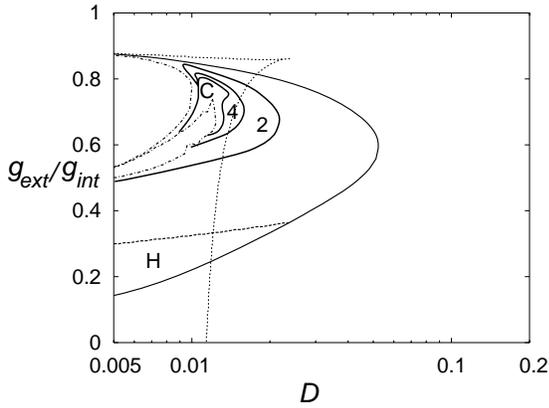
Figure 6: The areas where the periodic solutions with cycle 2 or 4, or the chaotic solutions exist are roughly sketched, and they are labeled "2", "4", and "C", respectively. In the area labeled "H", there exists the anomalous high-frequency synchronization.

of the probability flux and the raster plots for such a synchronization are shown in Figure 7. As shown in Figure 7B, it is observed that the frequencies of the excitatory neurons are very high, and their patterns of synchronization are hardly seen. It seems that this high-frequency synchronization does not correspond to the physiological observations because the periods of the physiologically observed periodic firings are much longer than the typical pulse width of a neuron. Thus, we call this high-frequency synchronization as the anomalous high-frequency synchronization. The anomalous high-frequency synchronization is realized because the probability flux J_E of the excitatory neurons always takes large values. A condition for the existence of the anomalous high-frequency synchronization is obtained as follows. Generally, if the product $\langle J_X(t)\rangle\Delta$ of the time-average $\langle J_X(t)\rangle$ of the probability flux and the pulse width Δ takes a value larger than 1, the neurons in the ensemble X continue to fire. With our parameters, the pulse width Δ is about 5. Thus, the excitatory neurons continue to fire if an inequality $\langle J_X(t)\rangle > 0.2$ is satisfied. In the area labeled "H" in Figure 6, this inequality is satisfied, and the anomalous high-frequency synchronization is observed.

Before closing this section, let us consider the dependence of the exponentially coupled network on the synaptic time constants κ_E and κ_I. The bifurcation sets for $\kappa_E = \kappa_I = 0.1$, $\kappa_E = \kappa_I = 0.5$, and $\kappa_E = \kappa_I = 3.0$ are shown in Figure 8. The boundaries of the areas where the periodic solution with cycle 2 or the chaotic solution exists are roughly sketched. The periodic solutions with larger cycles also exist for the
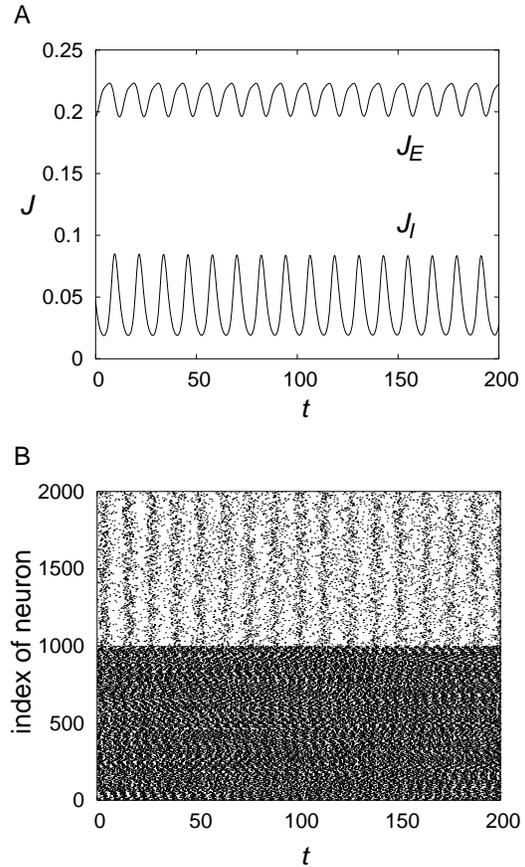
Figure 7: The anomalous high-frequency synchronization. (A) Flows of the probability flux and (B) the raster plots for the finite system with $N_E = N_I = 1000$ for $D = 0.014$, $g_{ext}/g_{int} = 0.3$, and $g_{int} = 3.5$.

parameters of Figure 8C, but we neglect them because those areas are very narrow. Moreover, the area where the anomalous high-frequency synchronization exists is also shown. As shown in Figure 8A, for small κ_E and κ_I, the structure of the bifurcation set is almost identical with that of the pulse-coupled network. This is because equation 4.1 reduces to $I_{XY}(t) = g_{XY}J_Y(t)$ in the limit of $\kappa_E, \kappa_I \rightarrow 0$, and it is equivalent to the interaction term of the pulse-coupling in equation 3.1. As shown in Figures 8B and C, when κ_E and κ_I are increased, the two homoclinic bifurcation lines merge, and the periodic solutions with n cycles and the chaotic solutions appear. Moreover, it is also observed that the area where the synchronized firings exist becomes narrower along the D-axis by the increase of κ_E and κ_I. In other words, the synchronized firings are more easily obtained for short synaptic decay time κ_E and κ_I. Note that the change of κ_E and κ_I does not affect the positions of equilibrium points because the
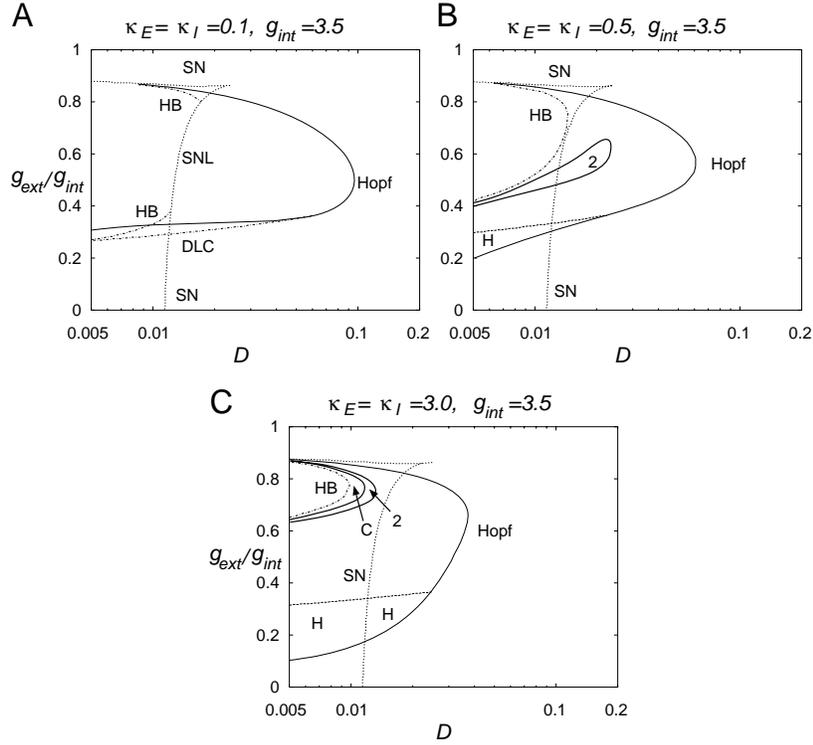
Figure 8: The bifurcation sets of the exponentially coupled network for (A) $\kappa_E = \kappa_I = 0.1$, (B) $\kappa_E = \kappa_I = 0.5$, and (C) $\kappa_E = \kappa_I = 3.0$. The internal coupling strength g_{int} is fixed at $g_{int} = 3.5$. The boundaries of the areas where the periodic solution with cycle 2 or the chaotic solution exist are rough sketches. Moreover, the areas where the anomalous high-frequency synchronization exists are also shown.

equilibrium of 4.1 is independent of κ_Y. Thus, if g_{ext}, g_{int}, and D are fixed, the firing rate or probability flux of the equilibrium point is kept constant with the change of κ_Y. However, the stability of equilibrium states depends on κ_E and κ_I, so the position of the Hopf bifurcation line changes.

5   Alpha-coupling   and   double exponential coupling

In the limit of $N_Y \to \infty$, the coupling term $I_{XY}(t)$ for the network with the alpha-coupling is approximated as (Gardiner, 1985)

$$I_{XY}(t) \quad = \quad g_{XY} \int_{-\infty}^{t} dt' \alpha(t - t'; \kappa_Y) J_Y(t'), \quad (5.1)$$

$$\alpha(t; \kappa) \quad \equiv \quad \frac{t}{\kappa^2} \exp\left(-\frac{t}{\kappa}\right), \quad\quad (5.2)$$

and it satisfies the differential equations written as

$$\dot{I_{XY}}(t) \quad = \quad -\frac{1}{\kappa_Y}(I_{XY} - I_{XY}^{(0)}), \quad\quad (5.3)$$

$$\dot{I_{XY}^{(0)}}(t) \quad = \quad -\frac{1}{\kappa_Y}(I_{XY}^{(0)} - g_{XY} J_Y), \quad\quad (5.4)$$

where

$$I_{XY}^{(0)}(t) \quad = \quad g_{XY} \int_{-\infty}^{t} dt' e(t - t'; \kappa_Y) J_Y(t'), (5.5)$$

$$e(t; \kappa) \quad \equiv \quad \frac{1}{\kappa} \exp\left(-\frac{t}{\kappa}\right). \quad\quad (5.6)$$

By integrating the Fokker-Planck equations with equations 5.3 and 5.4, the behavior of the network with the alpha-coupling can be analyzed.

On the other hand, for the network with the double exponential coupling, the coupling term $I_{XY}(t)$ can be approximated as

$$I_{XY}(t) \quad = \quad \frac{1}{\kappa_{1Y} - \kappa_{2Y}}(\kappa_{1Y} I_{XY}^{(1)} - \kappa_{2Y} I_{XY}^{(2)}), (5.7)$$

$$I_{XY}^{(1)}(t) \quad = \quad g_{XY} \int_{-\infty}^{t} dt' e(t - t'; \kappa_{1Y}) J_Y(t'), (5.8)$$

$$I_{XY}^{(2)}(t) \quad = \quad g_{XY} \int_{-\infty}^{t} dt' e(t - t'; \kappa_{2Y}) J_Y(t'), (5.9)$$

8

in the limit of $N_Y \to \infty$. And $I_{XY}^{(1)}(t)$ and $I_{XY}^{(2)}(t)$ satisfy the differential equations

$$\dot{I_{XY}^{(1)}}(t) = -\frac{1}{\kappa_{1Y}}(I_{XY}^{(1)} - g_{XY}J_Y), \quad (5.10)$$

$$\dot{I_{XY}^{(2)}}(t) = -\frac{1}{\kappa_{2Y}}(I_{XY}^{(2)} - g_{XY}J_Y). \quad (5.11)$$

By integrating the Fokker-Planck equations with equations 5.7, 5.10 and 5.11, the behavior of the network with the double exponential coupling can be analyzed.

Following the above procedures, bifurcation sets of the network with the alpha-coupling or the double exponential coupling are shown in Figure 9. Figure 9A shows the result for the alpha-coupling with $\kappa_E = \kappa_I = 1$, and Figures 9B and C show the results for the double exponential coupling with $\kappa_{1E} = \kappa_{1I} = 3$ and $\kappa_{2E} = \kappa_{2I} = 1$, and $\kappa_{1E} = \kappa_{1I} = 1$ and $\kappa_{2E} = \kappa_{2I} = 0.5$, respectively. The internal coupling strength g_{int} is fixed at $g_{int} = 3.5$. In Figure 9D, the corresponding parameter values are plotted in the $(\kappa_{1Y}, \kappa_{2Y})$ plane. By comparing Figures 9A and B, the effect of the decay time of the synaptic interaction can be summarized. Similarly to the results for the exponential coupling in Figure 8, with the increase of the decay time, the area where the synchronized firings exist becomes narrower along the D-axis. By comparing Figures 9A and C, the effect of the rise time can be summarized. Unlike the decay time, it is observed that the change of the rise time does not give a large effect on the overall bifurcation structure of the network.

We perform more detailed analyses about the dependence of the bifurcation structure on the synaptic time constants. We focus only on the large D, and consider the Hopf bifurcation observed when varying the synaptic time constants $\kappa_1 \equiv \kappa_{1E} = \kappa_{1I}$ and $\kappa_2 \equiv \kappa_{2E} = \kappa_{2I}$ for fixed D, g_{ext} and g_{int}. As stated in the previous section, the change of synaptic time constants affects the stability of the equilibrium points, but it does not affect the firing rate of each ensemble. The Hopf bifurcation lines observed when varying the synaptic time constants are shown in Figure 10. Typically, as shown in Figure 10A, the Hopf bifurcation takes place by decreasing the synaptic decay time κ_1, and the synchronized firings appear. This is because the area for the synchronized firings widens along the D-axis with the decrease of κ_1 as shown in Figure 8. On the other hand, as shown in Figure 10A, its dependence on the synaptic rise time κ_2 is not uniform. The Hopf bifurcation takes place with the change of κ_2 only when the synaptic decay time κ_1 is appropriately chosen. It is also observed that the synchronized firings appear even with the increase of κ_2.

Moreover, as shown in Figure 10B, there exist parameter values where long synaptic time constants
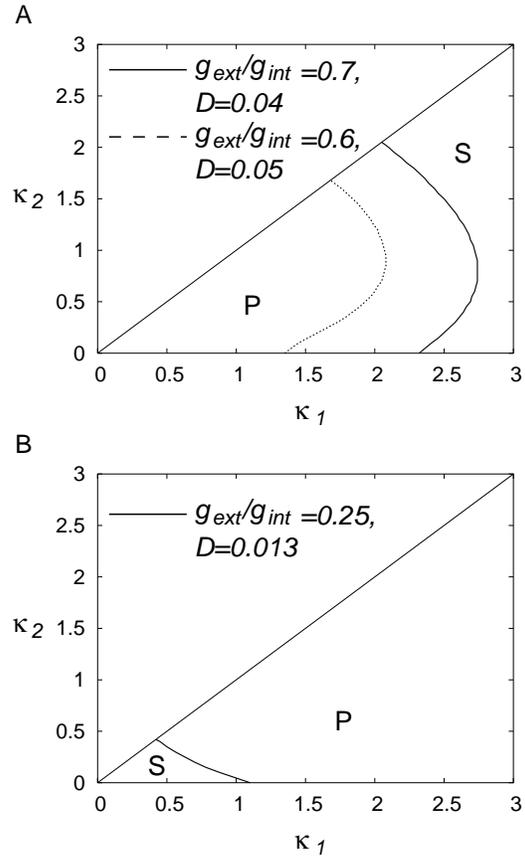
Figure 10: The Hopf bifurcation observed when varying the synaptic time constants for (A) $g_{ext}/g_{int} = 0.7$ and $D = 0.04$, $g_{ext}/g_{int} = 0.6$ and $D = 0.05$, and (B) $g_{ext}/g_{int} = 0.25$ and $D = 0.013$. The internal coupling strength g_{int} is fixed at $g_{int} = 3.5$. For (A), the synchronized periodic firings exist for short decay time κ_1, and, for (B), the synchronized periodic firings exist for long decay time κ_1. The synchronized state is stable in the area labeled "P", and the asynchronous state is stable in the area labeled "S".

cause the synchronized firings. This is because the area for the synchronized firings slightly widens along the g_{ext}-axis with the increase of κ_1 as shown in Figure 8. However, these synchronized firings are anomalous high-frequency synchronization, so this phenomenon might not have a physiological correspondence.

6 Conclusions and discussions

On the synchronized firings in the networks of class 1 excitable neurons with excitatory and inhibitory connections, their dependences on the forms of interactions are analyzed. As the forms of interactions, we
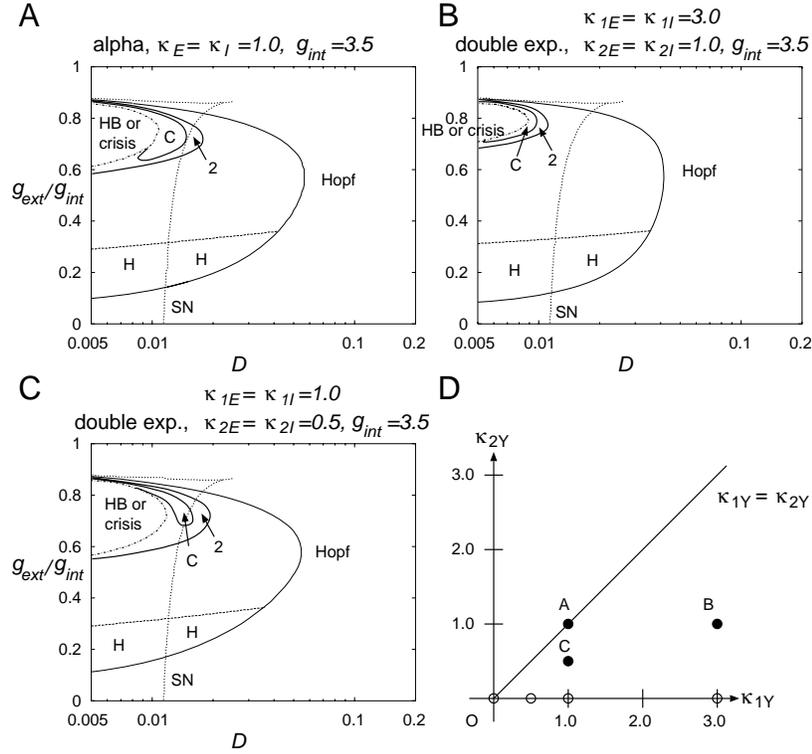
Figure 9: The bifurcation sets of the network with the alpha-coupling or the double exponential coupling. (A) alpha-coupling, $\kappa_E = \kappa_I = 1$. (B) double exponential coupling, $\kappa_{1E} = \kappa_{1I} = 3$ and $\kappa_{2E} = \kappa_{2I} = 1$. (C) $\kappa_{1E} = \kappa_{1I} = 1$ and $\kappa_{2E} = \kappa_{2I} = 0.5$. The internal coupling strength g_{int} is fixed at $g_{int} = 3.5$. (D) The chosen parameters are plotted in the $(\kappa_{1Y}, \kappa_{2Y})$ plane. The filled circles denote the parameters investigated in this figure, and the open circles denote the parameters treated in the previous sections.

treat the double exponential coupling and the interactions derived from it in some limiting cases, namely, the pulse-coupling, the exponential coupling, and the alpha-coupling, and investigate the dependence of the bifurcation structure on the rise time and the decay time of interactions.

By investigating the dependence of the solutions on the external connection strength g_{ext} and the noise intensity D, various synchronized firings are observed such as the synchronized periodic firings, the synchronized chaotic firings, and the anomalous high-frequency synchronization. The decay time κ_1 of the synaptic potential affects the bifurcation structure of the synchronized firings on the (D, g_{ext}) plane. With the decrease of κ_1, the area showing the synchronized firings widens along the D-axis. In other words, the synchronized firings are more easily obtained for a short synaptic decay time. It is also found that a relatively large value of κ_1 is required to observe the synchronized chaotic firings. The dependence of the overall bifurcation structure on the synaptic rise time κ_2 is weaker than that on κ_1.

In the analysis of synchronization in neural systems, the average firing rate of the ensemble is often fixed by regulating the constant input to the network (e.g., see Hansel and Mato (2003)). With such a procedure, it is possible to separate the effects of the firing rate and the other parameters on the bifurcation structure. In our model, the firing rate corresponds to the probability flux, and such a fixation of the firing rate is not performed in our analysis, namely, the value of the firing rate varies dependent on parameters g_{ext}, g_{int}, and D. Thus, our bifurcation sets reflect the effect of both the firing rate and the other parameters. However, when g_{ext}, g_{int}, and D are fixed, the firing rate of the equilibrium point takes a constant value. Thus, the effect of the firing rate is eliminated in the bifurcation set in the (κ_1, κ_2) plane (Figure 10).

Let us consider the effect of the time scale of the synaptic interaction on the synchronized firings. In the networks of self-oscillating excitatory neurons with alpha-couplings, it is known that the perfectly synchronized state is unstable (van Vreeswijk, 1996; van Vreeswijk, Abbott, and Ermentrout, 1994). In such

10

a network, the asynchronous state is stable for long synaptic time scales, and the partially synchronized state is stabilized for short synaptic time scales (van Vreeswijk, 1996). The synchronization observed in our noisy network would correspond to their partial synchronization, and, similarly to their results, the short synaptic time scale facilitates the synchronization in our network (see Figure 10A). It is noticeable that the synchronous state is stabilized even for long synaptic times in some parameter range (see Figure 10B). This effect can be understood by considering the overall bifurcation structure. However, this synchronous state corresponds to the anomalous high-frequency synchronization, so this phenomenon might not have a physiological correspondence. As for the rise time of the synaptic interaction, it is known that a pair of self-oscillating excitatory leaky integrate-and-fire neurons with exponential couplings shows the perfect synchronization although the network with alpha-couplings only shows the partial synchronization or the anti-phase synchronization (van Vreeswijk, Abbott, and Ermentrout, 1994). Moreover, for a pair of self-oscillating excitatory neurons with double exponential couplings, it is also known that the short rise time widens the parameter range where the partial synchronization is observed (Hansel, Mato, and Meunier, 1995). These results suggest that the short rise time facilitates the synchronization in the small network. However, our results show that the rise time of the synaptic interaction gives smaller effects on the overall bifurcation structure than that of the decay time. It might be because our network contains very large number of neurons, and the effect of a single pulse is scaled as $\sim N_X^{-1}$ ($X = E$ or I) and negligible. In such a network, the bifurcation structure might be determined by the characteristic time scale of the synaptic input $I_{XY}(t)$. In our configuration, the decay time is longer than the rise time ($\kappa_1 \geq \kappa_2$), so it is dominant in $I_{XY}(t)$.

Let us consider the roles of inhibition. In our network, the synchronized firings are not observed without inhibitory neurons (see bifurcation set at $g_{ext} = 0$), and it might be because our network is composed of excitable neurons. Although the period of the firings of networks of self-oscillating excitatory neurons is typically determined by the period of a single neuron, it can take various values depending on the parameters in the network of excitable neurons with excitatory and inhibitory connections. Typically, the period is long around the saddle-node on limit cycle bifurcation and the homoclinic bifurcation, and it is short around the Hopf bifurcation. Note that the period of the firings near the Hopf bifurcation can take large values if the activities of excitatory and inhibitory ensembles are balanced and weakly synchronized periodic firings are realized (Kanamaru and Sekine, 2004).

In the analysis of the pulse-coupled network, it is found that its bifurcation structure is similar to that of the network with the waveform-coupling written by equation 2.8 (Kanamaru and Sekine, 2003). The width of the pulse which is injected to the next neuron with the waveform-coupling is as large as $\Delta \sim 5$, and the width of the interaction of the pulse-coupled neuron is infinitesimal. Thus, this similarity seems to be strange. This contradiction might be explained as follows. In the network with the waveform-coupling or the pulse-coupling, each neuron has its characteristic time scale determined by (τ_E, a) or (τ_I, a), and, by the coupling, the additional characteristic time scale is not introduced to the network because the interaction with the waveform-coupling has the same characteristic time scale as the neuron, and the interaction with the pulse-coupling does not have a characteristic time scale. On the other hand, in the network with the other couplings such as the exponential coupling, a new characteristic time scale of the synapse is introduced to the network, so its dynamics becomes complex.

Hoppensteadt and Izhikevich considered weakly connected networks of class 1 neurons which are close to the saddle-node bifurcation point, and derived a canonical model which is described by phase variables connected with the pulse-coupling (Hoppensteadt and Izhikevich, 1997; Izhikevich, 1999). Because of the closeness to the bifurcation point, the characteristic time scale of the neuron is long, and the characteristic time scale of the coupling becomes relatively short. Thus, the pulse-coupling is justified in the canonical model. The behavior of this canonical model is expected to be similar to that of our pulse-coupled active rotators. On the other hand, when the neuron is away from the bifurcation point, the approximation with the pulse-coupling does not hold, so the couplings such as the double exponential coupling might be required. In such a network, the synchronized firings appear mainly through the Hopf bifurcation or the homoclinic bifurcation, and the synchronized periodic firings with large cycles and the synchronized chaotic firings are typically observed in a wide range of parameters. This ubiquity of the chaotic firings might suggests the importance of chaos in the brain dynamics.

In the present paper, for simplicity, we treated only the case where the time constants of the excitatory neurons and the inhibitory neurons are identical. Kanamaru and Sekine (2004) treated a network with the waveform-coupling which has different time constants $\tau_E = 1$ and $\tau_I = 2$, and it was found that its dynamics is more complex than that of the net-

work with $\tau_E = \tau_I = 1$. Moreover, the weakly synchronized periodic firings which are often observed in the physiological experiments (Gray and Singer, 1989; Buzsáki et al., 1992; Fisahn, Pike, Buhl, and Paulsen, 1998) are also observed in the network with $\tau_E = 1$ and $\tau_I = 2$. The physiological neurons have many characteristic time scales such as those of the various ion channels and the synaptic interactions, and it is known that the excitatory neurons and the inhibitory neurons have different values of time constants. Thus, it would be important to find dominant characteristic time scales in the physiological system and to incorporate it to the theoretical model.

A Numerical integration of the Fokker-Planck equation

In this section, we give a method for the numerical integration of Fokker-Planck equations 2.9 and 2.10. Two densities given by equations 2.13 and 2.14 are 2π-periodic functions of θ_E and θ_I, respectively, so they can be expanded as

$$n_E(\theta_E, t) = \frac{1}{2\pi}$$
$$+ \sum_{k=1}^{\infty} (a_k^E(t)\cos(k\theta_E) + b_k^E(t)\sin(k\theta_E)), \text{(A.1)}$$
$$n_I(\theta_I, t) = \frac{1}{2\pi}$$
$$+ \sum_{k=1}^{\infty} (a_k^I(t)\cos(k\theta_I) + b_k^I(t)\sin(k\theta_I)), \quad \text{(A.2)}$$

and, by substituting them, 2.9 and 2.10 are transformed into a set of ordinary differential equations $\dot{\boldsymbol{x}} = \boldsymbol{f}(\boldsymbol{x})$ where $\boldsymbol{x} = (a_1^E, b_1^E, a_1^I, b_1^I, a_2^E, b_2^E, a_2^I, b_2^I, \cdots)^t$,

$$\frac{da_k^{(X)}}{dt} = -\frac{k}{\tau_X}(1 + I_X)b_k^{(X)} + \frac{ak}{2\tau_X}(a_{k-1}^{(X)} - a_{k+1}^{(X)})$$
$$- \frac{k^2 D}{2\tau_X^2} a_k^{(X)}, \quad \text{(A.3)}$$

$$\frac{db_k^{(X)}}{dt} = \frac{k}{\tau_X}(1 + I_X)a_k^{(X)} + \frac{ak}{2\tau_X}(b_{k-1}^{(X)} - b_{k+1}^{(X)})$$
$$- \frac{k^2 D}{2\tau_X^2} b_k^{(X)}, \quad \text{(A.4)}$$

$$I_E \equiv I_{EE} - I_{EI}, \quad \text{(A.5)}$$
$$I_I \equiv I_{IE} - I_{II}, \quad \text{(A.6)}$$
$$a_0^{(X)} \equiv \frac{1}{\pi}, \quad \text{(A.7)}$$
$$b_0^{(X)} \equiv 0, \quad \text{(A.8)}$$

$k \geq 1$, and $X = E$ or I. These ordinary differential equations are numerically integrated with the forth-order Runge-Kutta algorithm.

Acknowledgement

References
Abbott, L. F., and van Vreeswijk, C. (1993) Asynchronous states in networks of pulse-coupled oscillators. *Physical Review E*, 48, 1483–1490.

Börgers, C., and Kopell, N. (2003). Synchronization in networks of excitatory and inhibitory neurons with sparse, random connectivity. *Neural Computation*, 15, 509–538.

Brunel, N. (2000). Dynamics of sparsely connected networks of excitatory and inhibitory spiking neurons. *Journal of Computational Neuroscience*, 8, 183–208.

Buzsáki, G., Horváth, Z., Urioste, R., Hetke, J., and Wise, K. (1992). High-frequency network oscillation in the hippocampus. *Science*, 256, 1025–1027.

Ermentrout, B. (1996). Type I membranes, phase resetting curves, and synchrony. *Neural Computation*, 8, 979–1001.

Fisahn, A., Pike, F. G., Buhl, E. H., and Paulsen, O. (1998) Cholinergic induction of network oscillations at 40Hz in the hippocampus in vitro *Nature*, 394, 186–189.

Gardiner, C. W. (1985). *Handbook of Stochastic Methods*, Berlin: Springer-Verlag.

Gerstner, W., and Kistler, W. (2002) *Spiking Neuron Models*, Cambridge: Cambridge University Press.

Golomb, D., and Ermentrout, G. B. (2001). Bistability in pulse propagation in networks of excitatory and inhibitory populations. *Physical Review Letters*, 86, 4179–4182.

Gray, C. M. (1994). Synchronous oscillations in neuronal systems: mechanisms and functions.

Journal of Computational Neuroscience, 1, 11–38.

Gray, C. M., and Singer, W. (1989). Stimulus-specific neuronal oscillations in orientation columns of cat visual cortex. *Proceedings of the National Academy of Sciences of USA*, 86, 1698–1702.

Guckenheimer, J., and Holmes, P. (1983). *Nonlinear Oscillations, Dynamical Systems, and Bifurcations of Vector Fields* New York: Springer.

Hansel, D., and Mato, G. (2003). Asynchronous states and the emergence of synchrony in large networks of interacting excitatory and inhibitory neurons. *Neural Computation*, 15, 1–56.

Hansel, D., Mato, G., and Meunier, C. (1995) Synchrony in excitatory neural networks. *Neural Computation*, 7, 307–337.

Hoppensteadt, F. C., and Izhikevich, E. M. (1997). *Weakly Connected Neural Networks*, New York: Springer.

Izhikevich, E. M. (1999) Class 1 neural excitability, conventional synapses, weakly connected networks, and mathematical foundations of pulse-coupled models. *IEEE Transactions on Neural Networks*, 10, 499–507.

Kanamaru, T., and Sekine, M. (2003). Analysis of globally connected active rotators with excitatory and inhibitory connections using the Fokker-Planck equation. *Physical Review E*, 67, 031916.

Kanamaru, T., and Sekine, M. (2004). An analysis of globally connected active rotators with excitatory and inhibitory connections having different time constants using the nonlinear Fokker-Planck equations. *IEEE Transactions on Neural Networks*, 15, 1009–1017.

Kuramoto, Y. (1984). *Chemical Oscillations, Waves, and Turbulence*, Berlin: Springer.

Kuramoto, Y. (1991). Collective synchronization of pulse-coupled oscillators and excitable units. *Physica D*, 50, 15–30.

Kurrer, C., and Schulten, K. (1995). Noise-induced synchronous neuronal oscillations. *Physical Review E*, 51, 6213–6218.

Mirollo, R. E., and Strogatz, S. H. (1990). Synchronization of pulse-coupled biological oscillators. *SIAM Journal of Applied Mathematics*, 50, 1645–1662.

Ott, E., (1993). *Chaos in Dynamical Systems*, New York: Cambridge University Press.

Press, W.H., Flannery, B.P., Teukolsky, S.A., and Vetterling, W.T. (1988). *Numerical Recipes in C*, Cambridge University Press, New York.

Sakaguchi, H., Shinomoto, S., and Kuramoto, Y. (1988). Phase transitions and their bifurcation analysis in a large population of active rotators with mean-field coupling. *Progress of Theoretical Physics*, 79, 600–607.

Sato, Y. D., and Shiino, M. (2002) Spiking neuron models with excitatory or inhibitory synaptic couplings and synchronization phenomena. *Physical Review E*, 66, 041903.

Shinomoto, S., and Kuramoto, Y. (1986). Phase transitions in active rotator systems. *Progress of Theoretical Physics*, 75, 1105–1110.

Tanabe, S., Shimokawa, T., Sato, S., and Pakdaman, K. (1999). Response of coupled noisy excitable systems to weak stimulation. *Physical Review E*, 60, 2182–2185.

Tsodyks, M., Mitkov, I., and Sompolinsky, H. (1993). Pattern of synchrony in inhomogeneous networks of oscillators with pulse interactions. *Physical Review Letters*, 71, 1280–1283.

van Vreeswijk, C. (1996) Partial synchronization in populations of pulse-coupled oscillators. *Physical Review E*, 54, 5522–5537.

van Vreeswijk, C., Abbott, L. F., and Ermentrout, G. B. (1994). When inhibition not excitation synchronizes neural firing. *Journal of Computational Neuroscience*, 1, 313–321.

van Vreeswijk, C., and Sompolinsky, H. (1996). Chaos in neuronal networks with balanced excitatory and inhibitory activity. *Science*, 274, 1724–1726.